Simple empirical model of the oceanic point spread function

Kenneth J. Voss

The point spread function (PSF) is an important property for predicting beam propagation and imaging system performance. Measurements of the PSF in three different locations (Pacific Ocean, Tongue of the Ocean, and Sargasso Sea) are presented. These measurements are used to validate extensive laboratory measurements [S. Q. Duntley, "Underwater Lighting by Submerged Lasers and Incandescent Sources," SIO Ref. 71-1, Scripps Institution of Oceanography, U. California, San Diego (1971)]. In all three locations a simple exponential expression describes the angular variation of the PSF in the 4–100-mrad range. The exponent in this relationship has a simple location specific dependence on attenuation length and the ratio of the absorption to beam attenuation coefficient. These relationships can be used to predict the PSF for an arbitrary path length. *Key words:* Ocean optics, point spread function, light scattering.

I. Introduction

The seawater point spread function (PSF) is an important parameter for many problems of underwater imaging and transmission.[1] Its mathematical equivalent,[2] the beam spread function (BSF), is important in beam propagation. In theory, the very small angle scattering phase function can be derived from the PSF using the techniques of Wells.[3] This portion of the scattering phase function is very hard to measure by other methods. Measurement of the PSF in the ocean, although important, has previously been reported for only a single location,[2] and very few reported measurements of the small angle scattering phase function exist.[4] Duntley reported extensive measurements of the BSF on simulated ocean water in a laboratory tank.[5] But with the exception of measurements performed in lake water, these were not validated with field measurements. Finally, the degree of variation in the small angle scattering phase function of the ocean, and hence the PSF, is virtually unknown. We thus began a program to measure the PSF in varied oceanic environments to determine the variability of this important parameter.

Mertens and Replogle[2] define the PSF(θ,R) as the apparent radiance of an unresolved Lambertian source at the position (0,0) normalized to source intensity. In this definition R is the distance between the source and detector, and θ refers to the angle between the axis of the source and the direction of view. This quantity has units of m^{-2}. In more physical terms, the PSF can be thought of as the image of an unresolved cosine source obtained with a camera and point source at opposite ends of the desired range. If there were no scattering, the PSF would be a δ-function in the center of the camera image. Because of scattering, the image of the point source is blurred, and this blurring is equivalent to the PSF. The BSF(θ,R) is similarly defined as the normalized irradiance distribution on a spherical surface of radius R centered on the transmitter. These definitions are illustrated in Fig. 1. By invoking the time independent reciprocity relationships of the electromagnetic radiation the PSF(θ,R) and BSF(θ,R) can be shown to be equivalent.[2]

The angular region that is of most interest in the PSF (or BSF) for imaging problems is of the order of 1 mrad, while minimum interesting ranges are usually of the order of 10 m. Most techniques to measure the PSF require precise alignment between the source and detector. When the measurements are required *in situ*, and in many different water types, this alignment is difficult or impossible to maintain. A measurement technique developed by Honey[6] avoids these problems. By use of a point source (a flashlamp) and a camera directed toward this point source, the PSF distribution measurement is contained in a single image frame. The problem of alignment is reduced to understanding the transformations relating the object

The author is with University of Miami, Physics Department, Coral Gables, Florida 33124.
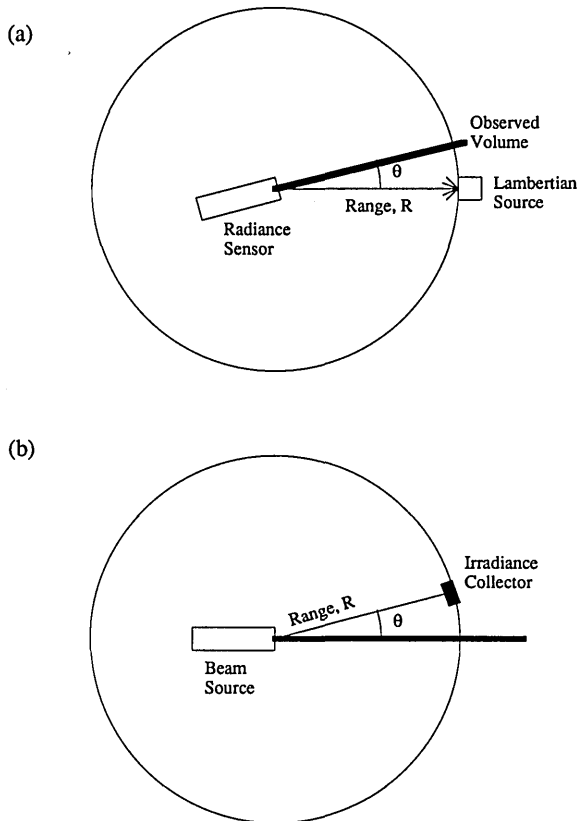
(a)

(b)

Fig. 1. Illustration of PSF (a) and BSF (b) definitions. These illustrations show the geometry of the measurement along with the similarity of the two measurements.

space to the image plane. This method also allows measurement of the PSF over longer ranges rather than extrapolating a small distance measurement to large distances. Details of the system design and calibration procedures for our camera system are described elsewhere.[7] The important facts for this analysis are the camera angular resolution (0.6 mrad in water) and the spectral response of the system (centered at 500 nm with a bandpass of 10 nm).

The data were obtained in two modes: fixed separation (or range) between the camera and flashlamp and varied separation. The first mode is useful for obtaining profiles of the PSF through the water column. This is arranged by locking the flashlamp at a given distance below the camera on the hydrowire and then fixing the camera to the wire. This allows the separation to be maintained almost exactly. The second mode allows the variation of the PSF with the range to be determined. This is arranged by locking the flashlamp to the hydrowire and allowing the camera to slide freely (with a separate support member) on the hydrowire. Keeping both units on the same wire helps to ensure that the flashlamp will be in the field of view of the camera even at large wire angles. The shadowing caused by the wire can be neglected since it obstructs an insignificant portion of the solid angle of the image.

As mentioned previously, Duntley has reported ex-

tensive measurements of the BSF in laboratory tank tests with simulated ocean water. In these laboratory tests the scattering and absorbing properties of the water were controlled with the addition of dyes and scattering agents (Nigrosin dye and Rexall Aluminox in this case). This allowed widely varying optical parameters to be measured in a controlled manner. However, the applicability of these measurements to the open ocean has not been demonstrated.

Duntley's measurements resulted in an empirical relationship of the beam spread vs angle given by the expression

$$\text{BSF}(\theta) = \frac{E(\theta)}{P} = \frac{10(A - C)\theta^B}{2\pi r^2 \sin\theta}, \tag{1}$$

where $A = 1.260 - 0.375 \, (cr)^{[0.710+0.489(a/c)]} - [1.378 + 0.053(c/a)] \, 10^{-cr[0.268+0.083(c/a)]}$, $B = 1 - 2(10^{-D})$, $C = \frac{1}{3}\{[(\theta/F)^{3/2} + 1]^{2/3} - 1\}$, $D = cr[0.018 + 0.011(c/a) + 0.001725cr]$, and $F = [13.75 - 0.501c/a] - [0.626 - 0.357c/a]cr + [0.01258 + 0.00354c/a](cr)^2$.

In these expressions $E(\theta)$ is the irradiance measured off-axis, P is the beam power, θ is the angle (in degrees) with respect to the unscattered collimated light, c is the beam attenuation coefficient, r is the range, and a is the absorption coefficient. The absorption coefficient is the loss in power of a beam, due to absorption, per meter, while the beam attenuation is the total loss in power of a beam, due to both absorption and scattering, per meter.[8] These relationships detail the variation of the BSF with the absorption coefficient. An advantage of the laboratory experiments is the ability to measure the absorption coefficient accurately, which at this time is difficult to measure *in situ* in the ocean.

III. Data

The field data were collected at three locations, the Sargasso Sea (SS), Tongue of the Ocean (TOTO), Bahamas, and coastal Pacific Ocean (PO). The hydrodynamic structures of the SS and TOTO stations were very different from the PO station, and this difference was evident in the optical properties of the water column.[9] Representative beam attenuation profiles are displayed in Fig. 2 for these locations. The most important feature is the relative homogeneity of the SS and TOTO stations compared with the PO station. The maximum in beam attenuation at ~30 m was reflected in the profiles of the PSF.

Three PSF measurements from the PO data set are shown in Fig. 3. The measured distribution is, strictly speaking, the convolution of the PSF with the light source radiance pattern. The central region, from 0 to ~2 mrad in these cases, is the blurred image of the source. The region between 4 and 100 mrad is the region for which the finite size of the source has little effect on the measured distribution; hence the PSF measured is the true PSF. These data illustrate the variability of the PSF in the water column with variation in the optical properties. All three measurements were taken at the same range and location. However, the attenuation lengths were 4.6, 3.1, and 2.4 for the
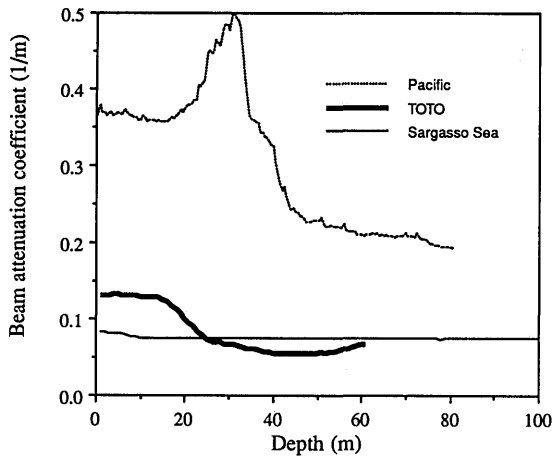
Fig. 2. Beam attenuation coefficient profiles from each location at ~500 nm. These profiles illustrate the differences in water column structure at these station locations, particularly the structure evident in the Pacific Ocean station.
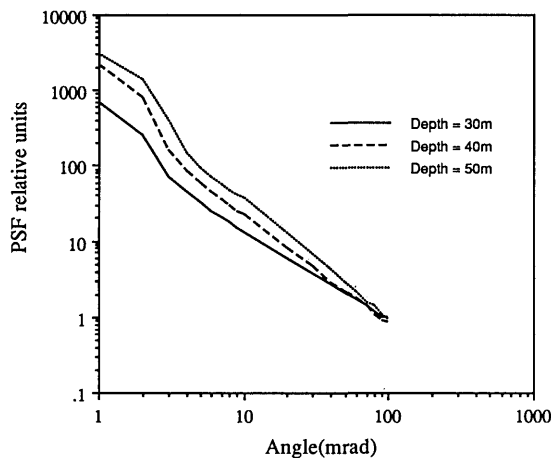

Fig. 4. BSF calculated from the empirical formula. This formula was derived from a series of laboratory measurements.[5] Parameters chosen were $cr = 4$, $a/c = 0.1$.

Fig. 3. PSF vs angle, showing the variability of the PSF with depth in an inhomogeneous water column, specifically the Pacific Ocean station. These data sets were taken at the same location within a period of 4 min. The variation is due to the structured water properties in this location; τ was 4.6, 3.1, and 2.4 for the 30-, 40-, and 50-m depths, respectively. The range was kept constant.

Fig. 5. The m vs τ calculated with the empirical formula.

30-, 40-, and 50-m depths, respectively. The difference in attenuation lengths were due to the structure of the beam attenuation profile. As can be seen the slope of the PSF varies inversely with attenuation length. The variation in optical properties in the measurement path is taken into account when calculating the attenuation length.

An important feature of the PSF is that it appears to be almost linear on the $\log(\text{PSF}) - \log(\theta)$ graph in the region between 4 and 100 mrad. This linearity implies a functional relationship of

$$\text{PSF}(\theta) = B_1\theta^{-m}, \qquad (2)$$

where B_1 is a constant and $-m$ is the slope of $\log(\text{PSF})$ vs $\log(\theta)$. In the three locations analyzed, the accuracy of this fit varied slightly due to differences in the exact
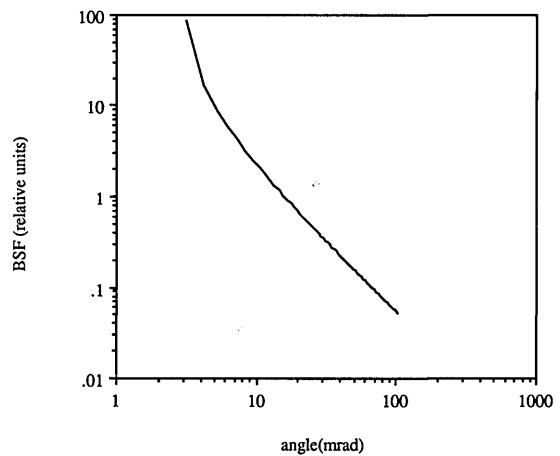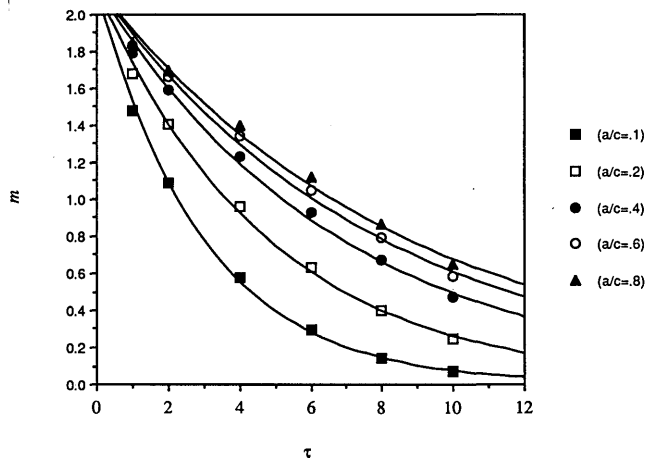
curvature of the measured PSF. The accuracy of the relationship was best with the PO stations where the average error of the prediction using the above equation was 10% (when m was fit to the individual data sets). The error for the SS and TOTO stations were 13 and 14%, respectively, while that for the combined data set was 13%.

The empirical relationships derived by Duntley, while explicitly more complicated, can also be fit by a function of the same form over the angular range considered (4–100 mrad). The calculated BSF for a specific cr and a/c is shown in Fig. 4. These calculations were performed for various attenuation lengths ($cr = 1$, 2, 4, 6, 8, 10) and absorption to attenuation ratios (a/c = 0.1, 0.2, 0.4, 0.6, 0.8). Each calculated data set was fit with an equation of the form given above, and the resulting m terms for each a/c were plotted against the attenuation length. These are illustrated in Fig. 5. The in situ data were also analyzed in a similar fashion. The factor cr used was the integrated attenuation coefficient between the camera and flashlamp τ defined by
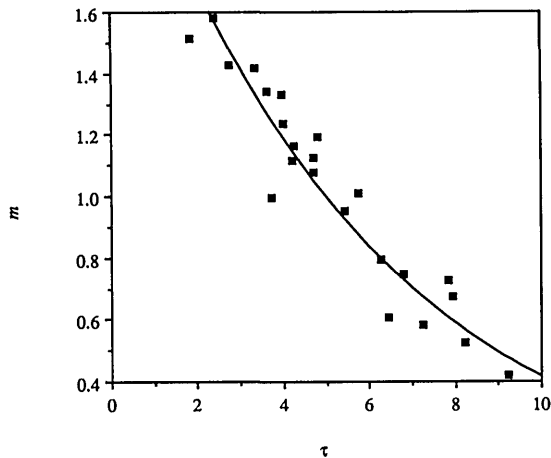
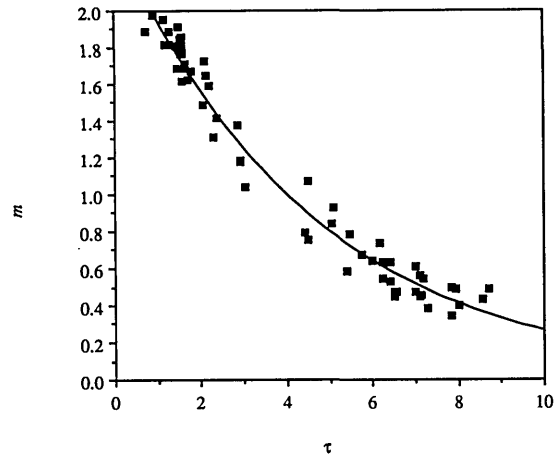Fig. 6. The m vs τ derived from the coastal Pacific Ocean data set.

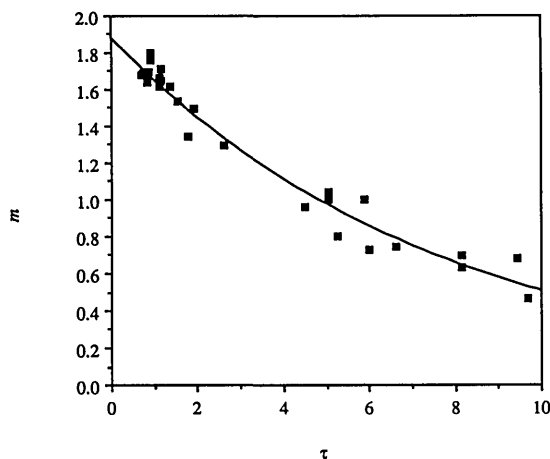Fig. 8. The m vs τ derived from the TOTO data set.

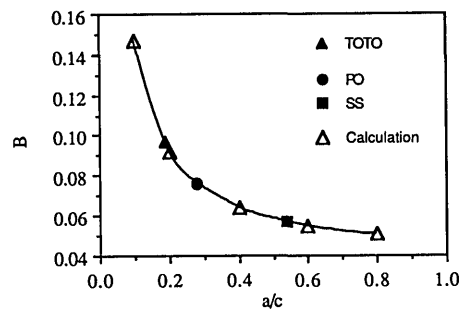Fig. 7. The m vs τ derived from the Sargasso Sea data set.

Fig. 9. The B vs a/c for calculated values. Also illustrated are the B terms for the field measurements.

Table I. Regressions for the Field Measurements of the Slope of the PSF(m) vs Attenuation Length (τ)

Location	A	B	r^2
Pacific Ocean	0.076	2.40	0.905
Sargasso Sea	0.057	1.88	0.964
TOTO	0.097	2.44	0.959

Note: The functional form was measured to be $m = A \times 10^{(-B\tau)}$.

$$\tau = \int_{z_1}^{z_2} c(z)dz/\cos\psi, \qquad (3)$$

where z_1 is the camera depth, z_2 is the flashlamp depth, $c(z)$ is the beam attenuation, dz is the incremental depth, and ψ is the observed angle of the hydrowire with the vertical. The ψ adjusts $(z_2 - z_1)$ to obtain the absolute range (in the measurements reported here $\psi = 0$). Thus, for each PSF measurement, τ was calculated using measurements of the beam attenuation profile (SS and TOTO measurements were provided by Smart[10]). Figures 6–8 illustrate the dependence of m on τ for each location. As can be seen they follow the same form as the empirical calculations. The scatter in the relationship between m and τ could be caused by several factors. The beam attenuation profiles used to derive τ were the closest in time and space to the PSF measurements but were not exactly contemporaneous. The error in the determination of m was determined to be ±0.3. The uncertainty in the camera and flashlamp depths was approximately ±0.2 m, or ±0.02–0.04 attenuation lengths. And finally the a/c varies to some extent with depth in the Pacific Ocean stations.

At large distances, the radiance field due to a point source in a scattering medium will become totally diffuse. At this point the PSF measured will be independent of angle; thus m will approach 0. Using this boundary condition a functional relationship of slope vs attenuation length of the form $A*10^{-B\tau}$ was assumed. The field data for each location and the calculated data for each a/c were fit to equations of the above form. Figure 9 illustrates the dependence of the B parameter with a/c for the calculations. The derived B values for the experimental data have been placed on the same figure. This analysis would predict average a/c ratios for the SS, TOTO, and PO locations to be 0.5, 0.25, 0.1, respectively. Measurements of a/c were available in the PO stations,[11] and the value obtained by these analyses falls within the range of measured values. Absorption measurements were not available for the other locations; thus these predicted a/c values cannot be verified.

The constant A varies with location in the experimental data as evidenced in Table I. In the empirical

relations this A was almost constant, 2.158 ± 0.003, over the entire range of a/c ($0.1 \leq a/c \leq 0.8$) calculated. This constant may be dependent on the scattering phase function of the water or on the exact angular response of the detector and receiver. The empirical relations were based on measurements which had a constant light scattering phase function determined by the Aluminox. They also had the same receiver and detector through the series of experiments. Our measurements had the same receiver and detector for the series of measurements. However, the phase function was probably location specific. This seems to indicate that the variations in A were due to the scattering phase function variability.

While this variability of A makes it impossible to determine the PSF(θ) for all locations independent of experimental measurement, the empirical relationships are still useful. If measurements of the PSF(θ) for several attenuation lengths exist for the desired location or water type, these may be used to determine the a/c (B) and A. A may be used to calculate the PSF(θ) for other attenuation lengths by adding an offset to τ given by

$$cr = \tau - \log(A/2.158)/B. \tag{4}$$

Thus the input parameters for the empirical relationship would be the a/c determined either through direct measurement, or though the relationship with B, and cr as given above.

III. Conclusions

These measurements confirm that the laboratory measurements of the BSF have the same form as the measured PSF in the open ocean. A simple linear form for the variation of log(PSF) with log(θ) is shown to fit both the experimental field data and the empirical equation in the 4–100-mrad range. While these relationships do not show the differences in curvature between locations which the measurements illustrate, they permit simple approximations of the PSF for specific attenuation lengths to be determined. The empirical relationship, derived from the laboratory measurements with accurately measured a values, can be used to estimate a/c for the field data. Further work is being performed to analyze the curvature differences in hopes of relating this to variations in the small angle scattering function.

References

1. B. L. McGlamery, "Computer Analysis and Simulation of Underwater Camera System Performance," SIO Ref. 75-2, Scripps Institution of Oceanography, U. California, San Diego (1975).
2. L. E. Mertens and F. S. Replogle, Jr., "Use of Point Spread and Beam Spread Functions for Analysis of Imaging Systems in Water," J. Opt. Soc. Am. 67, 1105–1117 (1977).
3. W. H. Wells, "Theory of Small Angle Scattering," in *Optics of the Sea*, AGARD Lect. Ser. 61 (NATO, 1973).
4. T. J. Petzold, "Volume Scattering Functions for Selected Ocean Waters," SIO Ref. 72-78, Scripps Institution of Oceanography, U. California, San Diego (1972).
5. S. Q. Duntley, "Underwater Lighting by Submerged Lasers and Incandescent Sources," SIO Ref. 71-1, Scripps Institution of Oceanography, U. California, San Diego (1971).
6. R. C. Honey, "Beam Spread and Point Spread Functions and Their Measurement in the Ocean," Proc. Soc. Photo-Opt. Instrum. Eng. 208, 242–248 (1979).
7. K. J. Voss and A. L. Chapin, "Measurement of the Point Spread Function in the Ocean," Appl. Opt. 29, 3638–3642 (1990).
8. A. Morel and R. C. Smith, "Terminology and Units in Optical Oceanography," Mar. Geod. 5, 335–349 (1982).
9. K. J. Voss, "Variability of the Point Spread Function in the Water Column," Proc. Soc. Photo-Opt. Instrum. Eng. 1302, 355–362 (1990).
10. J. Smart, Applied Physics Laboratory, Johns Hopkins U., Laurel, Md. 20707 (unpublished data, 1990).
11. K. J. Voss, "Use of the Radiance Distribution to Measure the Optical Absorption Coefficient in the Ocean," Limnol. Oceanogr. 34, 1614–1622 (1989).